Progress In Electromagnetics Research C, Vol. 173, 1–8, 2026

PIER C

(Received 7 June 2026, Accepted 24 July 2026, Scheduled 25 August 2026)

Accurate Modelling of the Nonlinear Magnetic Restoring Force and the Electromechanical Transduction Coefficient in an Electromagnetic Vibration Energy Harvester

Merwan Hebbache, Naamane Mohdeb*, Hocine Bouchekhou, Nabil Ikhlef, Hicham Allag, and Abdelghani Kimouche

L2EI Laboratory, Department of Electrical Engineering, Jijel University, Algeria

ABSTRACT: Electromagnetic harvesters based on magnetic levitation have emerged as particularly attractive systems owing to their contactless suspension, low mechanical damping, and inherently nonlinear stiffness behavior, which are suited to low-frequency ambient excitation. The investigated harvester consists of a levitating magnet suspended between two fixed outer magnets via repulsive magnetic forces, with a pickup coil converting oscillatory motion into electrical energy under base excitation. The primary source of difficulty in this system is the nonlinear magnetic restoring force F_{mag} and electromechanical transduction coefficient γ, wich must be pre-characterized using semi-analytical or finite element methods before any solution can be attempted. Therefore, the accurate pre-characterization of both F_{mag} and γ is the essential foundation of the entire modelling process. A Fourier space semi-analytical approach is proposed and developed, transforming a three-dimensional magnetostatic problem into a computationally efficient one-dimensional spectral calculation without remeshing. The semi-analytical predictions were validated against COMSOL finite element simulations, and their strong mutual agreement confirmed the accuracy of the proposed method before embedding it into the motion's coupled nonlinear equations.

1. INTRODUCTION

The extensive utilization of wireless sensors and microelectronics for real-time information processing has become increasingly prominent in recent years. However, relying on traditional chemical batteries to power these devices reveals critical limitations, primarily their short operating lives, inconvenient regular recharging, and significant contribution to environmental pollution [1–8]. A promising approach to deal with these issues is directly capturing energy from ambient renewable resources, with vibrational energy representing one of the most widely available and exploitable sources in both industrial and natural environments. Numerous techniques have been thoroughly investigated for harvesting vibrational energy, including piezoelectric and electromagnetic transduction methods, each offering distinct advantages depending on target application and frequency range [9]. The electromagnetic energy harvesting systems based on magnetic levitation have emerged as particularly well-suited for self-sustaining technology, owing to their simple design, minimal maintenance requirements, and reliable autonomous functionality over prolonged duration [10]. The energy conversion mechanism relies on the electromechanical interaction between levitating magnets and adjacent coils, which are standard low-cost components, thereby reducing both manufacturing and maintenance costs. Nevertheless, achieving greater harvesting efficiency while maintaining structural simplicity remains a central challenge in the development of this class of devices, as improved performance typically requires supplementary magnets and coils, which increase system complexity.

The described system is an electromagnetic vibrational energy harvester based on magnetic levitation, in which a central floating magnet is suspended between two fixed outer magnets via repulsive magnetic forces, and a pickup coil positioned at the equilibrium zone converts relative oscillatory motion into electrical energy when the base is subjected to mechanical excitation $y(t)$ by a shaker. This architecture is particularly attractive for low-frequency ambient vibration harvesting because of its contactless suspension, low mechanical damping, and inherently nonlinear stiffness behavior.

Therefore, accurately determining both magnetic restoring force and flux linkage gradient is a foundational step in the design, optimization, and performance prediction of magnetically levitated electromagnetic energy harvesters [7–15]. Nonlinear magnetic restoring force is the most influential parameter in harvester dynamics, as it determines resonant frequency, oscillation amplitude, degree of nonlinearity, and bandwidth of the device. Without an accurate magnetic restoring force, neither frequency response nor output power can be reliably predicted, rendering any subsequent dynamic simulation physically meaningless.

The Fourier space approach [13] for computing the magnetic restoring force in ring magnet assemblies is important at several levels, spanning fundamental modelling accuracy, computational efficiency, and practical harvester design. The Fourier space method fills this gap by transforming the

* Corresponding author: Naamane Mohdeb (mohdeb.naamane@gmail.com).

doi:10.2528/PIERC26060705

three-dimensional magnetostatic problem into a tractable one-dimensional spectral calculation for each axial wavenumber and assembling the complete force curve in the full magnet travel range at a fraction of the computational cost of finite element analysis. Beyond efficiency, spectral decomposition provides genuine physical insight by revealing which spatial harmonics dominate the force at different inter-magnet separations, quantitatively explaining why simple approximations break down at short ranges, guiding the choice of spectral truncation needed for convergence. The approach also enables rapid parametric sweeps over the magnet geometry (inner radius, outer radius, axial length, and separation distance) because each geometric variation affects only the sinc spectrum and Bessel function arguments without requiring remeshing. To verify the accuracy of the semi-analytical force characterization, its predictions were benchmarked against COMSOL finite element solutions. The strong correspondence between the two sets of results confirms the validity of the approach and establishes a reliable foundation for integrating the characterized force into the coupled nonlinear equations of motion of the harvester. In summary, the Fourier space approach is important not only as a computational convenience but also as a foundational modelling tool that connects the physical geometry of ring magnets to nonlinear dynamics of the harvester through a mathematically rigorous, computationally efficient, physically transparent chain of calculations that neither purely analytical nor purely numerical methods can provide alone.

2. MAGNETO-MECHANICAL DIFFERENTIAL EQUATIONS

The dynamics of magnetically levitated electromagnetic vibration energy harvesters are governed by two mutually coupled differential equations, representing mechanical and electrical domains. Mathematically, the system is governed by a set of coupled magneto-mechanical differential equations [3] as follows:

$$\begin{cases} m \cdot \dfrac{d^2 z}{dt^2} + c \cdot \dfrac{dz}{dt} + F_{\text{mag}} + \gamma \cdot i + mg = -m \cdot \ddot{y} \\ L_{\text{coil}} \cdot \dfrac{di}{dt} + (R_{\text{load}} + R_{\text{coil}}) i(t) = \gamma \dfrac{dz}{dt} \end{cases} \tag{1}$$

where m is the mass of the levitating magnet; g is the gravitational acceleration; k is the spring constant, related to the harvester's resonant frequency; and c is the mechanical damping coefficient. Therefore, the total damping acting on the levitating magnet is the sum $(c + C_{\text{em}})$, and the maximum harvested power is achieved when the electromagnetic damping is tuned to equal the mechanical damping.

The most fundamental difficulty in this system is strong bidirectional coupling between harvester's mechanical and electrical subsystems. The primary source of difficulty in this system is the nonlinear magnetic restoring force F_{mag}, whose coefficients must be pre-characterized via semi-analytical or finite-element methods before any solution can be attempted. The electromechanical transduction coefficient $\gamma = \frac{d\varphi}{dz}$ is a nonlinear function of displacement, introducing parametric nonlinearity into both equations simultaneously through its appearance in the feedback force term γi and electromotive source term $\gamma \frac{dz}{dt}$. This displacement dependence renders the electromagnetic damping coefficient $C_{\text{em}} = \gamma^2/(R_{\text{load}} + R_{\text{coil}})$ state-dependent rather than constant, significantly affecting prediction of the harvested power. The bidirectional mechanical-electrical coupling, combined with the inductive phase lag introduced by $L_{\text{coil}} \frac{diC}{dt}$ and the gravitational equilibrium offset produced by mg, makes the system a genuinely challenging nonlinear dynamical problem that cannot be solved using standard linear techniques. The accurate determination of both F_{mag} and γ as continuous spatial functions of displacement constitutes the essential and indispensable foundation of the entire harvester modelling process. The coupled nonlinear equations of motion were solved numerically using the Runge-Kutta 4th/5th-order adaptive scheme through the MATLAB ode45 solver, which balances accuracy and step size.

3. MAGNETIC CALCULATION MODEL USING FOURIER SPACE APPROACH

The present formulation builds on the Fourier-space magnetostatic framework developed by Beleggia and co-workers [12–14], originally applied to nanoparticle interactions and demagnetization factors, which is here extended to compute the force and transduction coefficient of a magnet-coil levitation system.

3.1. Magnetostatic Energy

For modelling the magnetic field and levitation forces, the Fourier space approach is highly effective. It is much faster than finite element analysis (FEA) for optimization and provides a continuous solution for magnetic fields. The application of the Fourier-space approach to cylindrical ring magnets is considerably more demanding than to simpler geometries, and difficulties arise at every stage of the formulation, from field representation to force integration. The spring constant originates from the magnetic restoring forces, which are analytically

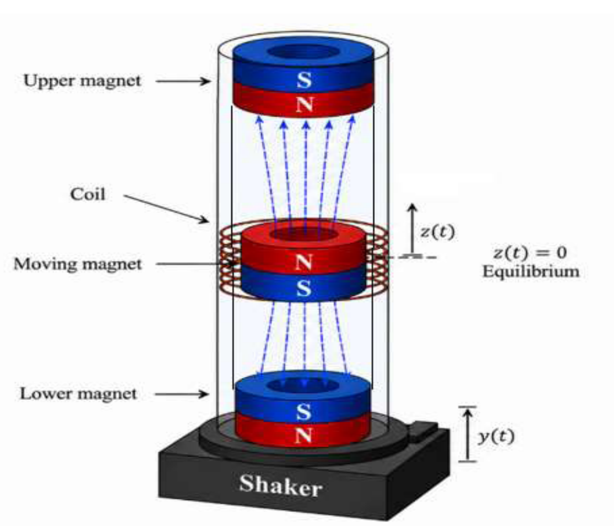

FIGURE 1. Schematic diagram of the electromagnetic vibrational energy harvester system.

determined by taking the spatial gradient of the magnetostatic energy within the system [13]:

$$E_m = -\frac{\mu_0}{2}\int_V \mathbf{H}(\mathbf{r})\cdot\mathbf{M}(\mathbf{r})\,d^3\mathbf{r} \tag{2}$$

where H, M, r, μ_0, and V are the magnetic field strength, magnetization, vector position in Cartesian space, permeability in free space, and volume, respectively.

Assuming cylindrical geometry, the system energy is derived using a shape function $D(r)$, a discontinuous function equal to unity inside the object and zero outside [14]. Now, the energy interaction between two particles is derived, whose shape functions are $D_i(r)$, magnetization states $m_i(r)$, and located at positions r_i, as shown in Fig. 2. The figure illustrates the relative positions of two magnetically interacting sources within the Fourier-space formulation, establishing the spatial reference framework on which the magnetostatic interaction energy is derived.

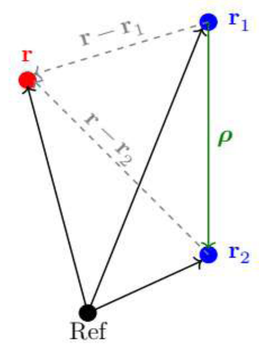

FIGURE 2. Relative position of two particles.

For the case of two bodies, the resulting magnetic-field strength and magnetization are the sum of each body's contribution [11]:

$$\mathbf{M}(\mathbf{r}) = \mathbf{M}_1(\mathbf{r}-\mathbf{r}_1)+\mathbf{M}_2(\mathbf{r}-\mathbf{r}_2) \tag{3}$$
$$\mathbf{H}(\mathbf{r}) = \mathbf{H}_1(\mathbf{r}_1)+\mathbf{H}_2(\mathbf{r}_2) \tag{4}$$

The magnetization $M(\mathbf{r})$ of a cylindrical magnet with uniform axial magnetization M_r is defined by the shape function. This geometric decomposition is essential for analytical formulation. In real space, the magnetization distribution of each magnet is expressed through its shape function as follows [12]:

$$\mathbf{M}(\mathbf{k}) = M_r\mathbf{D}(\mathbf{k}) \tag{5}$$

$$\mathbf{D}(\mathbf{k}) = \int \mathbf{D}(\mathbf{r})e^{-i\mathbf{k}\cdot\mathbf{r}}\,d\mathbf{r} \tag{6}$$

Because the system is source-free (no free currents), the relationship between H and M in the Fourier space is governed by the projection of the magnetization onto the wave vector **k**:

$$\mathbf{H}(\mathbf{k}) = -\frac{\mathbf{k}(\mathbf{k}\cdot\mathbf{M}(\mathbf{k}))}{k^2} \tag{7}$$

Substituting this into the flux density equation yields:

$$\mathbf{B}(\mathbf{k}) = \mu_0\left(-\frac{\mathbf{k}(\mathbf{k}\cdot\mathbf{M}(\mathbf{k}))}{k^2}+\mathbf{M}(\mathbf{k})\right) \tag{8}$$

The contribution of two magnetic sources in Fourier space [13]:

$$\mathbf{M}(\mathbf{k}) = \sum_{n=1}^{2} M_n\mathbf{D}_n(\mathbf{k})\hat{\mathbf{m}}_n e^{i\mathbf{k}\cdot\mathbf{r}_n} \tag{9}$$

where $\mathbf{D}_n(\mathbf{k})$ is the shape factor or distribution function in k-space related to the geometry of the magnet; $\hat{m}_n$ is the unit vector indicating the direction of magnetization; and $e^{ik\cdot r_n}$ is a phase shift term that accounts for the spatial position r_n of the magnet. The term $e^{ik\cdot r_n}$ is critical because it encodes the physical position r_n of each magnet in the model. Even if the two magnets are identical, their different positions in space result in different phase signatures in the Fourier space. Thus, the total magnetostatic energy of the two-source system in the Fourier space [14] is:

$$\begin{aligned} E_m \;=\; \frac{\mu_0}{16\pi^3}\int\frac{d^3\mathbf{k}}{\mathbf{k}^2}\Bigg(&\sum_{i=1}^{2}(\mathbf{M}_n(\mathbf{k})\cdot\mathbf{k})^2 \\ &+(\mathbf{M}_1(\mathbf{k})\cdot\mathbf{k})(\mathbf{M}_2(\mathbf{k})\cdot\mathbf{k})e^{i\mathbf{k}\cdot(\mathbf{r}_1-\mathbf{r}_2)} \\ &+(\mathbf{M}_1(\mathbf{k})\cdot\mathbf{k})(\mathbf{M}_2(\mathbf{k})\cdot\mathbf{k})e^{-i\mathbf{k}\cdot(\mathbf{r}_1-\mathbf{r}_2)}\Bigg) \end{aligned} \tag{10}$$

where the expression $E_{m,s} = \sum_{i=1}^{2}(\mathbf{M}_n(\mathbf{k})\cdot\mathbf{k})^2$ is the self-energy term. This represents the energy inherent to each magnet individually (the energy required to assemble magnet 1 and magnet 2 in isolation), and the expression $E_{m,i} = (\mathbf{M}_1(\mathbf{k})\cdot\mathbf{k})(\mathbf{M}_2(\mathbf{k})\cdot\mathbf{k})e^{i\mathbf{k}\cdot(\mathbf{r}_1-\mathbf{r}_2)}+(\mathbf{M}_2(\mathbf{k})\cdot\mathbf{k})(\mathbf{M}_1(\mathbf{k})\cdot\mathbf{k})e^{-i\mathbf{k}\cdot(\mathbf{r}_1-\mathbf{r}_2)}$ is the interaction energy term (Fig. 3). This is the most important part of our research. It represents the mutual energy between the two magnets. The two cross-terms in $E_{m,i}$ are complex conjugates of each other and represent the same physical interaction. Consequently, the magnetostatic interaction energy is given by [10]:

$$E_m = \frac{\mu_0}{8\pi^3}\left((\mathbf{M}_1(\mathbf{k})\cdot\mathbf{k})(\mathbf{M}_2(\mathbf{k})\cdot\mathbf{k})e^{i\mathbf{k}\cdot(\mathbf{r}_1-\mathbf{r}_2)}\right) \tag{11}$$

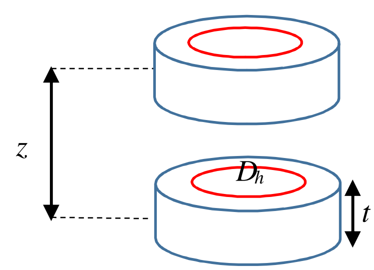

FIGURE 3. Scheme of the two interacting ring-shaped magnets.

The convolution of the magnetic fields, which is computationally intensive in the spatial domain, is simplified to an algebraic product in k-space:

$$E_m = \frac{\mu_0 M_1 M_2}{16\pi^3}$$
$$\mathcal{R}_e\left\{\int d^3\mathbf{k}\,D_1(\mathbf{k})D_2(\mathbf{k})(\hat{\mathbf{m}}_1\cdot\mathbf{k})(\hat{\mathbf{m}}_2\cdot\mathbf{k})e^{i\mathbf{k}\cdot(\mathbf{r}_1-\mathbf{r}_2)}\right\} \tag{12}$$

The shape functions represent the geometric distribution of the two ring magnets in the frequency domain. For a ring magnet with thickness t, outer radius r, and inner (hole) radius r_h, the function is defined as [13]:

$$D_1(\mathbf{k}) = \frac{2\pi t_1}{k_\perp}\mathrm{sinc}\left(\frac{t_1}{2}k_\perp\right)\left(r_1 J_1(k_\perp r_1) - r_{1h} J_1(k_\perp r_{1h})\right) \quad (13)$$

$$D_2(\mathbf{k}) = \frac{2\pi t_2}{k_\perp}\mathrm{sinc}\left(\frac{t_2}{2}k_\perp\right)\left(r_2 J_1(k_\perp r_2) - r_{2h} J_1(k_\perp r_{2h})\right) \quad (14)$$

where $k_\perp = \sqrt{k_x^2 + k_y^2}$ is the transverse component of the wave vector, and J_1 is the first-order Bessel function of the first kind, which accounts for the radial geometry. The resulting equation for the total potential energy of the system is [13]:

$$E_m = 4\pi\mu_0 M_1 M_2 r_1 r_2^2 \int \frac{dq}{q^2}\left[J_1\left(\frac{r_1}{r_2}q\right) - \frac{r_{1h}}{r_1}J_1\left(\frac{r_{1h}}{r_2}q\right)\right]$$

$$\left[J_1(q) - \frac{r_{2h}}{r_2}J_1\left(\frac{r_{2h}}{r_2}q\right)\right] \sinh\left(\frac{r_1}{r_2}\tau_1 q\right) \sinh(\tau_2 q) e^{-\xi q} \quad (15)$$

The spatial distribution is normalized using dimensionless parameters ξ_1 and ξ_2, which represent the relative distance to each magnetic source: $\xi_1 = \frac{z}{R_1}$, $\xi_2 = \frac{(d-z)}{R_2}$.

3.2. Repulsive Magnetic Force

By evaluating the gradient of the interaction energy, the derivation of the repulsive force is significantly simplified, as the spatial dependence is contained entirely within the exponential term. The resulting expression for the repulsive magnetic force between two ring magnets is formulated as:

$$F_m = -\nabla E_m$$

Considering a levitating magnet positioned at height z between a fixed bottom magnet and a fixed top magnet, the energy is expressed as [11-14]:

$$F_m = K_e r_2 \int \frac{dq}{q}\left[J_1\left(\frac{r_1}{r_2}q\right) - \frac{r_{1h}}{r_2}J_1\left(\frac{r_{1h}}{r_2}q\right)\right]$$

$$\left[J_1(q) - \frac{r_{2h}}{r_2}J_1\left(\frac{r_{2h}}{r_2}q\right)\right] \sinh\left(\frac{r_1}{r_2}\tau_1 q\right) \sinh(\tau_2 q) e^{-\xi q} \quad (16)$$

where $\alpha = t_1/2$, $\delta = t_2/2$, $t_1 = 2r_1\tau_1$, $t_2 = 2r_2\tau_2$, $q = r_2 k_\perp$, $dq = r_2 dk_\perp$, $z_{12} = r_2\xi$, $K_e = 4\pi\mu_0 M_1 M_2 r_1$.

In practical terms, this formula is used to calculate the axial restoring force or the coupling in electromagnetic levitation systems. Because it is an analytical integral rather than a finite element simulation, it allows much faster computation when optimizing system dimensions. This specific mathematical structure is common in electromagnetics for calculating interactions between non-contacting components, such as vibration energy harvesters and wireless power transfer systems.

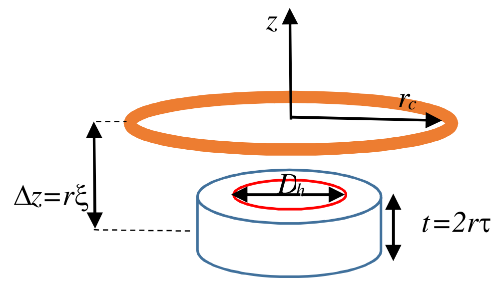

FIGURE 4. Dimensions and position of the permanent magnet and coil.

3.3. Magnetic Flux and Gradient of the Magnetic Flux

The magnetic flux from a levitating magnet through a coil must be calculated by considering both internal (inside the magnet) and external (outside the magnet) positions. When the magnet is inside (Fig. 4), the flux is determined by the magnetization $B = \mu_0(H + M)$; when outside, it depends only on the magnetic field intensity $B = \mu_0 H$. The magnetic flux φ through a single turn of the coil at a position z is defined by the surface integral of the magnetic field B over the area S enclosed by the coil:

$$\varphi = \iint_S B\, dS = \int_0^{2\pi}\int_0^{R_c} B_z(r,\theta,z)\, r\, dr\, d\theta \quad (17)$$

The induced magnetic flux φ through the coil is governed exclusively by the axial component B_z. The magnetic flux density B produced by the levitating permanent magnet was modeled using a spectral domain approach. In this framework, the field is expressed as the inverse Fourier transform of the magnet geometry and magnetization properties. For a magnet with remanent magnetization B_r and a geometric shape factor $D(\mathbf{k})$ in the Fourier space, the magnetic flux density outside the magnet volume (B_{out}) is given by [13, 14]:

$$B_{\text{out}} = -\frac{B_r}{8\pi^3}\int \frac{D(\mathbf{k})}{k^2}\mathbf{k}(\hat{\mathbf{m}}\cdot\mathbf{k})e^{i\mathbf{k}\cdot\mathbf{r}}\, d^3\mathbf{k} \quad (18)$$

$$B_{\text{in}} = -\frac{B_r}{8\pi^3}\int D(\mathbf{k})\left(\mathbf{k} - \mathbf{k}\frac{\hat{\mathbf{m}}\cdot\mathbf{k}}{k^2}\right)e^{i\mathbf{k}\cdot\mathbf{r}}\, d^3\mathbf{k} \quad (19)$$

The derivative of the flux with respect to time gives the induced electromotive force (EMF), which is directly proportional to the velocity of the magnet and the spatial gradient of the magnetic field. This can also be expressed as the product of the permanent magnet speed and the derivative of the flux with respect to the position:

$$\text{EMF} = -v_z\frac{d\varphi}{dz} = -v_z\gamma \quad (20)$$

Because the damping coefficient is a function of the flux gradient (γ), the magnetic flux profile of the levitating magnet relative to the coil must first be established. The magnetic flux for both cases, where the magnet is located inside or outside the coil, is obtained by evaluating the inverse Fourier transform of the spectral field distributions [11, 12]:

$$\varphi_{\text{in}} = 2\pi\mu_0 M_r r_c \int_0^\infty \frac{dq}{q} J_1\left(\frac{r_c}{r_p}q\right)$$

$$\left[r_p J_1(q) - r_h J_1\left(\frac{r_h}{r_p}q\right)\right]\left[1-\cosh(\xi q)e^{-\tau q}\right] \quad (21)$$

$$\varphi_{\text{out}} = 2\pi\mu_0 M_r r_c \int_0^\infty \frac{dq}{q} J_1\left(\frac{r_c}{r}q\right)$$
$$\left[r J_1(q) - r_h J_1\left(\frac{r_h}{r}q\right)\right]\sinh(\tau q)e^{-\xi q} \quad (22)$$

The EMF ($-v_z\gamma$) is generated as the magnet moves through the coil. According to Faraday's law, it is proportional to the rate of change of magnetic flux, which is directly related to the magnet's velocity (v_z). Depending on whether the coil is positioned above or below the magnet (or considering the interaction between the two faces of the ring), the induced voltage for a single loop of radius R_c is expressed as [14]:

$$\gamma_{\text{in}} = \nabla\varphi_{\text{in}} = 2\pi\mu_0 M_r r_c \int_0^\infty dq$$
$$\left(J_1(q) - \frac{r_h}{r_p}J_1\left(\frac{r_h}{r_p}q\right)\right) J_1\left(\frac{r_c}{r_p}q\right)\sinh(\xi q)e^{-\tau q} \quad (23)$$

$$\gamma_{\text{out}} = \nabla\varphi_{\text{out}} = 2\pi\mu_0 M_r r_c \int_0^\infty dq$$
$$\left(J_1(q) - \frac{r_h}{r_p}J_1\left(\frac{r_h}{r_p}q\right)\right) J_1\left(\frac{r_c}{r_p}q\right)\sinh(\tau q)e^{-\xi q} \quad (24)$$

The flux linkage exhibits strong position dependence relative to each individual loop within the coil. Consequently, conventional approximations, which often assume a uniform field across all N turns, frequently result in discrepancies when compared with experimental data. To achieve a higher fidelity, it is necessary to sum the individual contributions of each loop.

$$\text{EMF}_T = -\sum_{i=0}^{n}\sum_{j=0}^{n} v_z\gamma(r_{c_i}, z_j) \quad (25)$$

where r_{c0}, r_{cn} are the coil's radial boundaries, and z_0, z_n are the coil's axial boundaries.

By defining the coil via its physical boundaries, the model no longer treats the coil as a single point source or thin filament. Instead, it captures the flux gradient variations across thick windings.

4. RESULTS AND DISCUSSIONS

As shown in Fig. 1, a single coil is used to capture the magnetic-field variation induced by the relative motion between the magnet and coil. The harvester was built around three NdFeB N42 grade ring magnets sharing the same inner and outer diameters of 6 mm and 15 mm, respectively. The central levitating magnet is 5 mm long and floats with a 40 mm separation from each fixed magnet, while the two fixed outer magnets are slightly thicker at 6 mm in length and spaced 113 mm apart from each other, defining the total travel space available for the floating magnet. The pickup coil was wound with 26 AWG copper wire for 138 turns, has an inner diameter of 20 mm and an outer diameter of 25 mm, giving it a radial thickness of 2.5 mm and an axial length of 10 mm, and was positioned with a 35 mm separation from fixed magnets to ensure that it was precisely at the equilibrium zone where the flux gradient $d\Phi/dz$ and thus electromagnetic coupling were maximum. The harvester is subjected to a sinusoidal base excitation at a frequency of $f = 9$ Hz, corresponding to an angular frequency of $\omega = 2\pi f$, and a driving amplitude of $A = 4$ mm. The prescribed base displacement and velocity are given, respectively, by:

$$z(t) = -A\cos(\omega t) \quad (26)$$
$$v(t) = A\omega\sin(\omega t) \quad (27)$$

The permanent magnets are characterized by a remanent magnetization of 1.15 T. The mechanical dissipation of the levitating magnet is modeled via a damping coefficient $c = 0.10$, while the electrical circuit is characterized by a coil resistance $R_{\text{coil}} = 1.3\,\Omega$.

By considering magnetic properties, geometry, and coil arrangement, the new model analyzes factors such as the magnetic flux density, field gradients, and interactions between magnets and coils. This analysis aids in optimizing the magnet configuration and coil design for efficient energy conversion. Several important outputs can be investigated to assess this system's performance and effectiveness.

Figure 5 shows a COMSOL simulation of iso-lines (non-equipotential lines) of the magnetic vector potential around two coaxial ring magnets in a repulsive configuration, enclosed within a cylindrical tube. The non-uniform spacing of these iso-lines confirms the highly inhomogeneous and nonlinear nature of the magnetic field distribution produced by the two opposing ring magnets. Here, the software COMSOL was used to verify the derived analytical expression by calculating the repulsive force experienced by a levitating magnet as a function of its relative distance to the top and bottom magnets, as shown in Fig. 6. This repulsion zone is precisely where the floating magnet levitates in the harvester system, as the opposing magnetic forces from above and below create a single stable equilibrium at the center, thereby reinforcing the system's monostable nature. The magnetostatic problem was solved in COMSOL Multiphysics using magnetic fields with no current physics interface under a 2D axisymmetric formulation, exploiting the rotational symmetry of the magnet assembly. The computa-

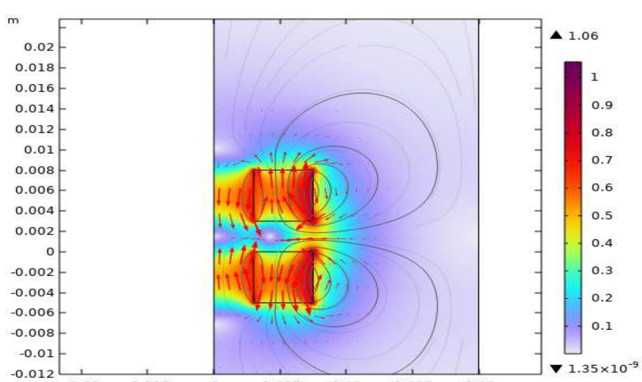

FIGURE 5. Vector potential simulation results between magnets.

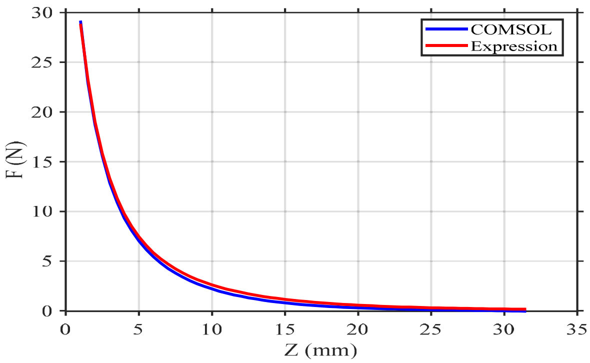

FIGURE 6. Magnetic repulsive force F (N) between two magnets as a function of their separation distance Z (mm).

tional domain was discretized using free triangular elements, refined near the magnet edges and coil region to resolve local field gradients, and truncated using an infinite-element domain of thickness to approximate the open-boundary condition, with magnetic insulation applied to the outer boundary.

Figure 6 compares the magnetic repulsive force between two magnets as a function of their separation distance Z, validating the analytical expression against a COMSOL numerical simulation. The two curves show excellent agreement across the full range, which validates that the analytical expression accurately captures the real magnetic behavior and can be confidently used in the dynamic equations of motion without requiring a full COMSOL solve at every step. Physically, the force behaves as a strongly nonlinear decaying function; at very close distances ($Z \to 0$), the repulsion force is extremely large (nearly 30 N), reflecting the intense field concentration observed in the simulations. As the separation increases, the force drops rapidly and asymptotically approaches zero beyond $Z \approx$ 25–30 mm, indicating that magnets barely interact at large distances.

Figure 7 shows the magnetic force acting on the middle floating magnet as a function of its displacement Z from equilibrium, again comparing the COMSOL simulation (blue line) with the analytical expression (black dots), with near-perfect agreement throughout. Unlike the previous plot, which showed a single repulsive interaction, this curve represents the combined effect of both fixed magnets acting simultaneously on the floating magnet. At $Z = 0$ (equilibrium), the net force

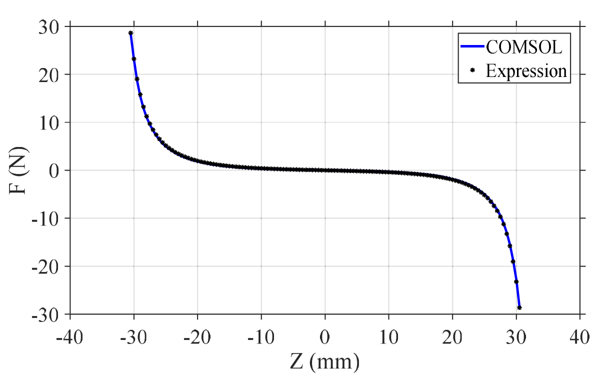

FIGURE 7. Magnetic repulsive force F (N) between two magnets as a function of their separation distance.

is exactly zero (the upper and lower repulsions are perfectly balanced), confirming the stable levitation point. When the magnet is displaced upward ($Z > 0$), the net force becomes negative (pushing back down), and when displaced downward ($Z < 0$), the force becomes positive (pushing back up); this is the classic signature of a restoring force, which is mathematically analogous to a nonlinear spring. Critically, the curve is antisymmetric about $Z = 0$ and has a characteristic S-shape, which reveals that the restoring force is strongly nonlinear. This nonlinear stiffness provides the harvester with a soft-spring behavior in the middle range and hardening behavior near the extremes. This force profile is the direct input to the harvester's motion equation, replacing the linear spring term kz with the nonlinear magnetic force F, and is essential for accurately predicting the dynamic response, bandwidth, and power output of the harvester.

Figure 8 shows the magnetic vector potential iso-line map of the electromagnetic energy harvester. Only the central magnet moves vertically inside the rectangular coil, whereas the two outer magnets remain fixed. As the central magnet oscillates, it changes the local flux distribution around it, thereby altering the total flux Φ threading the coil over time. This variation $d\Phi/dt$ induces an EMF in the coil, converting the mechanical vibration of the central magnet into electrical energy. The two fixed outer magnets act as magnetic bias sources, pre-loading the flux environment and amplifying the flux variation caused by the moving central magnet, which increases the induced EMF and improves harvesting efficiency compared with a single-magnet configuration.

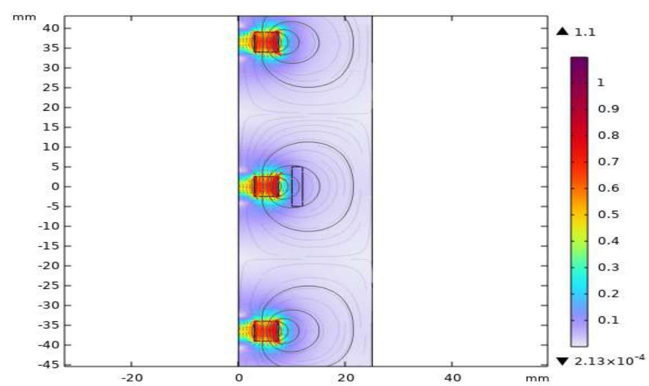

FIGURE 8. Vector potential simulation results for the interaction between the levitating magnet and the coil.

Figure 9 shows the spatial derivative of the magnetic flux through the coil as a function of the floating magnet displacement Z, comparing COMSOL with the analytical expression (dashed red line), with very good agreement. This profile directly defines the electromechanical coupling coefficient of the harvester and is critical for computing the damping force fed back onto the magnet, output voltage waveform, and the device's overall power conversion efficiency.

Figure 10 shows the total magnetic flux threading the coil as a function of floating magnet displacement Z, comparing COMSOL (black) to the analytical expression (red). A notable observation is that the red analytical expression decays more slowly than the black COMSOL curve at large displacements

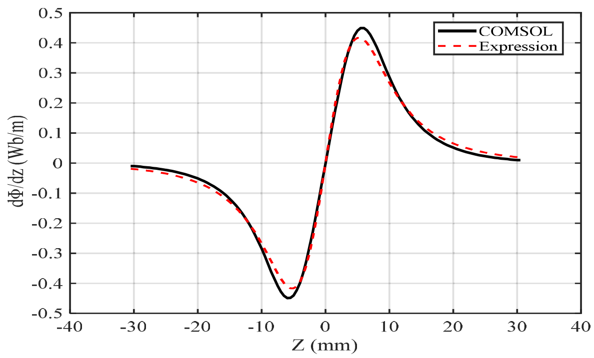

FIGURE 9. Gradient of the magnetic flux with respect to the position in an N-loop coil.

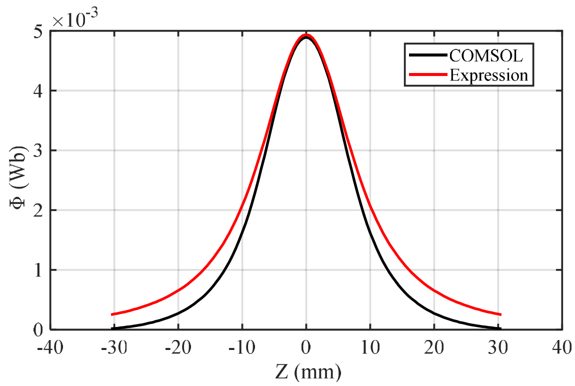

FIGURE 10. Magnetic flux with respect to the position in an N-loop coil.

(beyond ± 15 mm), indicating a slight overestimation of the flux at the tails, which is a common limitation of simplified analytical models that assume ideal dipole or uniform magnetization, while COMSOL captures the actual finite geometry of the magnets more accurately. This discrepancy is small but should be considered when modelling large-amplitude oscillations. Together, the $\Phi(Z)$ profile and its gradient $d\Phi/dz$ fully characterize the electromagnetic coupling of the harvester, providing all the information needed to compute the induced voltage, current, electrical damping force, and harvested power as functions of the magnet's dynamic position.

The induced electromotive force (EMF) (V) is a quasi-sinusoidal alternating signal oscillating between approximately $+0.35$ V and -0.35 V, revealing a slight asymmetry between positive and negative peaks. This asymmetry is physically meaningful as it reflects the nonlinear and non-uniform nature of the $d\Phi/dz$ profile observed earlier, where the positive and negative peaks were not perfectly equal, causing the magnet's upward and downward strokes to induce slightly different voltage amplitudes. The signal was periodic and stable, indicating the magnet oscillated in a steady-state limit cycle under continuous harmonic excitation from the shaker. The frequency of oscillation was approximately 9.5 Hz (approximately 19 cycles over 2 s), which is consistent with a low-frequency ambient vibration source, which is the regime that this type of magnetic levitation harvester is designed to exploit. A small phase difference is visible between COMSOL and analytical curves, which grows slightly over time, stemming from minor discrepancies

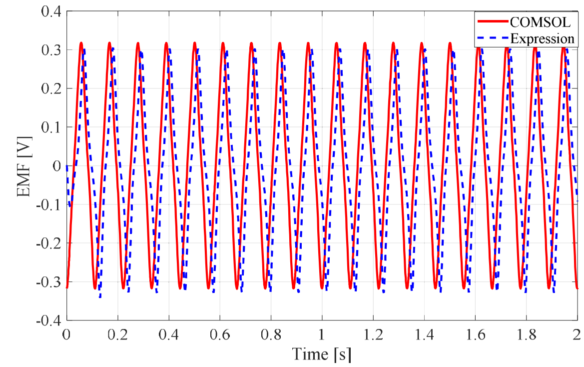

FIGURE 11. Induced EMF time signal (harvester output voltage).

in the flux model at large displacements noted in the previous $\Phi(Z)$ plot. Fig. 11 shows the induced EMF (V) generated by the harvester over time (0 to 2 s), comparing COMSOL against the analytical expression, with strong overall agreement in both amplitude and frequency.

In all figures, analytical expressions consistently match COMSOL results with high accuracy, demonstrating that the proposed mathematical model faithfully captured the harvester's nonlinear magnetic, mechanical, and electromagnetic behaviors. The semi-analytical approach evaluates EMF (V) through a one-dimensional spectral integral over the magnet's shape amplitude, requiring 10 s, compared to 1200 s for the corresponding COMSOL solve, which additionally requires mesh generation at each new geometric configuration. This validated model provides a reliable and computationally efficient framework for the device's dynamic analysis, performance prediction, and design optimization without requiring repeated costly FEM simulations.

5. CONCLUSION

This study presents a comprehensive analytical framework for modelling and characterizing an electromagnetic vibrational energy harvester based on magnetic levitation, with the Fourier-space approach, serving as the central methodological contribution. The Fourier-space method is highly effective in computing both the nonlinear magnetic restoring force and flux linkage gradient in the full displacement range, offering a physically transparent and mathematically rigorous alternative to purely numerical approaches. Its validation against COMSOL finite element simulations confirmed a strong agreement across all computed quantities. The nonlinear magnetic restoring force exhibited a characteristic antisymmetric S-shaped profile, confirming the monostable nature of the levitation system and its inherent soft-spring to hardening-spring transition, which is essential for broadband low-frequency energy harvesting. The electromechanical coupling coefficient, derived from the spatial gradient of the magnetic flux, was accurately reproduced analytically, enabling reliable prediction of the induced EMF, electrical damping, and harvested power. By replacing costly finite element solutions with semi-analytical integrals, the proposed model enables rapid parametric sweeps over the magnet geometry and coil configuration, making it a powerful tool for design optimization. The induced EMF output oscillated at approximately 9.5 Hz with a consistent amplitude, confirming the harvester's suitability for real-world low-frequency ambient vibration environments.

Overall, the validated coupled magneto-mechanical model establishes a solid, efficient foundation for predicting, analyzing, and optimizing the dynamic performance of magnetically levitated electromagnetic energy harvesters, paving the way for self-sustaining wireless sensing applications.

REFERENCES

[1] Mann, B. P. and N. D. Sims, "Energy harvesting from the nonlinear oscillations of magnetic levitation," *Journal of Sound and Vibration*, Vol. 319, No. 1-2, 515–530, 2009.

[2] Saha, C. R., T. O'donnell, N. Wang, and P. McCloskey, "Electromagnetic generator for harvesting energy from human motion," *Sensors and Actuators A: Physical*, Vol. 147, No. 1, 248–253, 2008.

[3] Covaci, C. and A. Gontean, "Piezoelectric energy harvesting solutions: A review," *Sensors*, Vol. 20, No. 12, 3512, 2020.

[4] Muscat, A., S. Bhattacharya, and Y. Zhu, "Electromagnetic vibrational energy harvesters: A review," *Sensors*, Vol. 22, No. 15, 5555, 2022.

[5] Dowlati, S., N. Kacem, and N. Bouhaddi, "Enhancing the performance of vibration energy harvesting based on 2 : 1 : 2 internal resonance in magnetically coupled oscillators," *Micromachines*, Vol. 16, No. 1, 23, 2025.

[6] Kecik, K., "Simultaneous vibration mitigation and energy harvesting from a pendulum-type absorber," *Communications in Nonlinear Science and Numerical Simulation*, Vol. 92, 105479, 2021.

[7] Sebald, G., H. Kuwano, D. Guyomar, and B. Ducharne, "Simulation of a Duffing oscillator for broadband piezoelectric energy harvesting," *Smart Materials and Structures*, Vol. 20, No. 7, 075022, 2011.

[8] Li, Z., L. Rong, A. Lan, M. Tang, and Y. Sun, "Design and experimental research of a track vibration energy harvester based on a wideband magnetic levitation structure," *Machines*, Vol. 14, No. 2, 225, 2026.

[9] Imbaquingo, C., C. Bahl, A. R. Insinga, and R. Bjørk, "A two-dimensional electromagnetic vibration energy harvester with variable stiffness," *Applied Energy*, Vol. 325, 119650, 2022.

[10] Jensen, T. W., A. R. Insinga, J. C. Ehlers, and R. Bjørk, "The full phase space dynamics of a magnetically levitated electromagnetic vibration harvester," *Scientific Reports*, Vol. 11, No. 1, 16607, 2021.

[11] Imbaquingo, C., C. Bahl, A. R. Insinga, and R. Bjørk, "Two-dimensional elliptically shaped electromagnetic vibration energy harvester," *Sensors and Actuators A: Physical*, Vol. 350, 114091, 2023.

[12] Beleggia, M., S. Tandon, Y. Zhu, and M. D. Graef, "On the magnetostatic interactions between nanoparticles of arbitrary shape," *Journal of Magnetism and Magnetic Materials*, Vol. 278, No. 1-2, 270–284, 2004.

[13] Beleggia, M., D. Vokoun, and M. D. Graef, "Demagnetization factors for cylindrical shells and related shapes," *Journal of Magnetism and Magnetic Materials*, Vol. 321, No. 9, 1306–1315, 2009.

[14] Beleggia, M. and M. D. Graef, "General magnetostatic shape–shape interactions," *Journal of Magnetism and Magnetic Materials*, Vol. 285, No. 1-2, L1–L10, 2005.

[15] Mohdeb, N., H. Allag, and T. Hacib, "A new approximation for calculating the attraction force in cylindrical permanent magnets arrays and cylindrical linear single-axis-actuator," *Progress In Electromagnetics Research C*, Vol. 91, 213–225, 2019.